JOURNAL OF CATALYSIS 131, 74–87 (1991)

# Chemical Modification of Catalyst Support for Enhancement of Transient Catalytic Activity: Nitric Oxide Reduction by Carbon Monoxide over Rhodium

BYONG K. CHO

*Physical Chemistry Department, General Motors Research Laboratories, Warren, Michigan 48090-9055*

Received November 6, 1990; revised April 24, 1991

A commercial ceria powder was chemically modified by doping with gadolinia in order to improve its oxygen storage/transport characteristics. The catalytic activity of Rh impregnated on this modified ceria support was measured and compared with those impregnated on conventional ceria or alumina support, using a packed-bed reactor and an isotopic reactant ($^{13}CO$) for the NO + CO reaction under both cycled- and steady-feed conditions. Results of transient pulse experiments indicated that the oxygen uptakes of both ceria and modified ceria are an order of magnitude greater than that of alumina. This work has demonstrated that the chemical modification of the ceria support can significantly enhance the catalytic activity of Rh for the NO + CO reaction under cycled feedstream conditions at high temperatures above 500°C. This enhancement of catalytic activity of Rh supported on the modified ceria is discussed in light of the oxygen storage and transport characteristics of the modified support. 

## INTRODUCTION

The reaction of NO with CO is a major reaction pathway for the removal of nitrogen oxides from automobile exhaust, and its elementary surface processes involve decomposition of NO to produce nitrogen and oxygen, and subsequent oxidation of CO by the resulting surface oxygen. Among the major ingredients of three-way catalysts Rh has been well recognized for its superior activity toward the NO reduction as well as CO oxidation compared with Pt and Pd. However, the current usage level of Rh in automobile catalytic converters is significantly higher than the mine ratio, raising serious concern about its price and availability in the future. Thus, extensive research efforts have been directed during the last decade toward the reduction or elimination of the Rh requirement in three-way catalytic converters without adversely affecting the overall converter performance (*1–5*).

Cerium oxide (or ceria) has been widely used as an additive ingredient in the automotive three-way catalytic converters for various reasons; it promotes the water–gas shift reaction (*6–9*), it stabilizes the dispersion of noble metals on alumina support (*9, 10*), and it stores and releases oxygen under net-oxidizing and net-reducing conditions, respectively (*6–9*). Recent studies by Oh and Eickel (*11*) and Oh (*12*) have shown that ceria added to $Rh/Al_2O_3$ can enhance the rate of both CO + $O_2$ reaction and CO + NO reaction under certain steady-state conditions. Among these different aspects of the role of ceria in supported noble metal catalysts, this paper focuses primarily on its oxygen storage capability when used as a catalyst support.

The idea of enhancing the catalytic activity of noble metals for NO decomposition by improving the oxygen storage/transport characteristics of the support material is relatively new (*13, 14*) even though the oxygen storage capability of ceria has been widely known in automobile exhaust catalysis



0021-9517/91 $3.00

(e.g., *6–9, 15, 16*). Previously we have shown that the activity of $Rh/Al_2O_3$ catalysts for NO decomposition deteriorates due to the accumulation of surface oxygen derived from the NO decomposition, and that the lifetime of $Rh/Al_2O_3$ catalysts for NO decomposition can be significantly extended by using an alternate support such as ceria, which has oxygen storage capacity greater than that of alumina (*13*). Since the surface oxygen in deactivated Rh catalysts can be removed by a reducing agent such as CO, we further examined the possibility that the catalytic activity of Rh may also be enhanced by using a ceria support instead of the traditional alumina support when CO and NO are alternately fed to the reactor. Indeed, a more recent study has convincingly demonstrated that a significant enhancement of NO conversion can be achieved during the cycled operation of the NO + CO reaction over $Rh/CeO_2$ compared with $Rh/Al_2O_3$ catalysts (*14*). This enhanced catalytic activity could be attributed to the ability of the ceria support to store a greater amount of oxygen during the cycled operation.

In view of the importance of oxygen storage capacity of ceria in influencing the transient catalytic activity of Rh, it is appropriate to examine the mechanism by which ceria can transport and store oxygen. The process of oxygen storage and transport in ceria can be described by the defect mechanism (*17, 18*), and there are two types of defects involved in this process. One is the intrinsic defects and the other is the extrinsic defects. The intrinsic defects are due to the oxygen anion vacancies created upon the reduction of ceria according to the redox process involving ceria:

$$CeO_2 + \delta R \rightleftharpoons CeO_{2-\delta} + \delta RO + \delta V_O, \quad (1)$$

where $R$ is a reductant, $RO$ is a gaseous product, and $V_O$ is an oxygen anion vacancy which may be charged either singly or doubly depending on the condition (*18*). The extrinsic defects are due to the oxygen anion vacancies created by the charge compensation effect of foreign cations which have a valence lower than that of the host cerium ions they substitute. For example, the doping reaction of ceria with trivalent cations can be written as

$$2 M_2O_3 + 3 Ce_{Ce} \rightarrow 4 M_{Ce} + 3 CeO_2 + 2 V_O, \quad (2)$$

where $M$ is the trivalent cation, $Ce_{Ce}$ is the Ce cation on the Ce site of the ceria lattice, $M_{Ce}$ is the trivalent cation on the Ce cation site in Kroger–Vink notation (*19*), and the oxygen vacancy is assumed to be doubly charged. To the best of our knowledge, the concept of the extrinsic oxygen vacancy has never been applied to catalyst design, even though the importance of oxygen storage and transport in automotive exhaust catalysis has long been recognized.

The role of aliovalent (i.e., divalent or trivalent) cation dopants in enhancing ionic conductivity in oxides of the fluorite structure such as ceria is well known (*20*); trivalent dopants generally produce a higher conductivity than divalent ones for the same dopant concentration (*21*). Ionic conductivity through ceria is due to the migration of these oxygen vacancies, and thus is a measure of oxygen mobility. Thus, the extrinsic defect mechanism suggests that the rate of oxygen transport as well as the capacity of oxygen storage can be enhanced by chemical modification of ceria through doping with cations of a lower valence. This idea led us to develop a new modified ceria support that contains extrinsic oxygen vacancies. In this work, the reactivity of Rh catalysts supported on this modified ceria is compared and contrasted with those supported on alumina or conventional ceria. It is demonstrated that the modified ceria can significantly enhance the catalytic activity of Rh for the NO + CO reaction above 500°C under cycled operating conditions.

## DESIGN OF MODIFIED CERIA SUPPORT

Ceria is generally added to automotive three-way catalysts as an oxygen storage

component (*6–9, 15, 16*). It has recently been shown, based on the principle of charge compensation (*20–24*), that ceria can be doped readily with trivalent cationic oxides ($M_2O_3$) to become a better oxygen conductor owing to newly created extrinsic oxygen vacancies. When we consider both intrinsic and extrinsic oxygen vacancies in the modified ceria support, the oxygen storage process of ceria can be written as

$$CeO_{2-\delta} \rightleftharpoons CeO_2 \rightleftharpoons CeO_{2+\delta'}, \qquad (3)$$

where $\delta$ represents the oxygen storage capacity due to the redox process while $\delta'$ represents an additional oxygen storage capacity due to the extrinsic oxygen vacancy. Thus, conventional ceria can have the oxygen storage capacity of $\delta$ while the modified ceria can have the oxygen storage capacity of $(\delta + \delta')$.

Obviously, the key question in designing a modified ceria support is the type and amount of the dopant to be incorporated into the ceria lattice. In choosing the type of trivalent cationic oxide for the purpose of enhancing oxygen storage and transport characteristics, we have taken into account the following facts.

1. Rare-earth oxides with a trivalent cation are known to be the best possible dopants for ceria because rare-earth elements can easily replace cerium on its regular site due to the closeness in their electronegativity to that of cerium (*20*).

2. The oxygen ion conductivity in the modified ceria depends strongly on ionic radius of the dopant (*22, 23, 25*), and the highest ionic conductivity can be obtained when the ionic radius of the dopant is the same as that of the host (*25*).

3. The structural integrity of the ceria lattice is best preserved if the lattice parameter of the dopant is the same as that of ceria and there is no variation in the lattice parameter after doping.

Based on the above considerations, we chose $Gd_2O_3$ as the best possible dopant for our purpose; Gd is one of the rare-earth elements, its ionic radius is very close to that of cerium, and the lattice parameter of $CeO_2$–$Gd_2O_3$ is almost the same as that of $CeO_2$ (*26*).

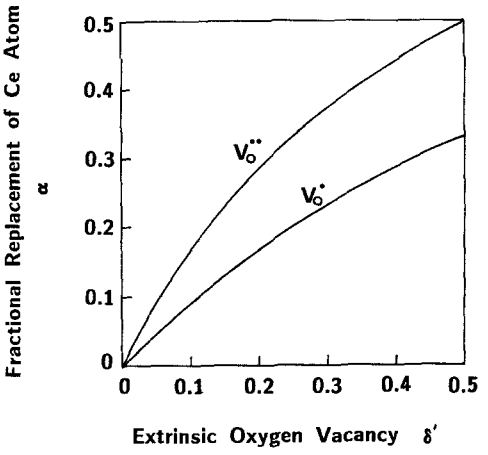


FIG. 1. Relation between the amount of dopant cation ($\alpha$) and the created extrinsic vacancy ($\delta'$) in ceria.

The solid-state reaction by which we want to modify $CeO_2$ can be written as

$$2(1-\alpha)\,CeO_2 + \alpha\,Gd_2O_3 \rightarrow 2\,Ce_{1-\alpha}Gd_\alpha O_{2-0.5\alpha} + \delta'\,V_O, \qquad (4)$$

where $Ce_{1-\alpha}Gd_\alpha O_{2-0.5\alpha}$ is the modified ceria designated as $CeO_2$-$a$, and $\delta'$ is a convenient representation of the created extrinsic oxygen vacancy in the modified ceria. According to the theory of defects (*19*), an oxygen vacancy is created for two $Gd^{+3}$ substituting two $Ce^{+4}$ in the $CeO_2$ lattice if the oxygen vacancy is doubly charged. This means

$$\delta' = \alpha/2(1-\alpha) \qquad (5)$$

for the doubly charged oxygen vacancies. Similarly, for the singly charged oxygen vacancies, one oxygen vacancy is created for each $Gd^{+3}$ substituting a $Ce^{+4}$ in the $CeO_2$ lattice, resulting in

$$\delta' = \alpha/(1-\alpha). \qquad (6)$$

It has been reported that the oxygen vacancies are predominantly doubly charged for small deviations from stoichiometry, while they are singly charged for large deviations from stoichiometry (*18*). Figure 1

shows the relation between the amount of dopant represented as the fraction of Ce atoms replaced by the dopant atoms ($\alpha$) and the created extrinsic oxygen vacancy ($\delta'$) in the modified ceria. The upper curve is for doubly charged oxygen vacancies and the lower is for the singly charged ones. Note that the number of oxygen vacancies increases monotonically with the amount of dopant.

We want to point out that, under transient operating conditions, the large number of oxygen vacancies alone does not necessarily translate into a large oxygen storage capacity unless the rate of oxygen uptake is sufficiently fast. That is, both a large number of oxygen vacancies and high anion mobility are two essential requirements for an efficient oxygen storage material. In choosing the right amount of the dopant, we must consider therefore the following effects of dopant concentration on the oxygen mobility.

1. Oxygen mobility increases with oxygen vacancy concentration, which increases with the amount of dopant.

2. The associative interaction between the dopant cation and the oxygen vacancy increases with the increasing amount of dopant, resulting in a reduced oxygen mobility (*24, 27*).

The above indicates that there is an optimum amount of dopant for maximum oxygen mobility. Since $\alpha$ cannot exceed 0.5 as shown in Fig. 1, there must be an optimum value of $\alpha$ between 0 and 0.5 for the maximum oxygen mobility; without further detailed analysis, we arbitrarily chose 0.2 for $\alpha$ in this work.

## EXPERIMENTS

### *Catalyst Preparation*

Three different supports were used in this study: $\gamma$-alumina ($Al_2O_3$), ceria ($CeO_2$), and modified ceria ($CeO_2$-*a*). In the modified ceria, the chemical modification of the ceria was achieved by forming a binary solid solution of ceria with gadolinia. The binary solid solution with the Ce-to-Gd atomic ratio of 4-to-1 was obtained by the heat treatment of a uniform mixture of fine powders of ceria and gadolinia smaller than 325 mesh. The heat treatment consisted of thermal fusion of the powdery mixture at 1400°C under atmospheric conditions (i.e., exposed to air at 1 atm pressure), followed by cooling to room temperature. The resulting binary solid solution was crushed, ground, and screened for 80–120 mesh sizes to be used as catalyst supports. X-ray diffraction analysis of the modified ceria confirmed that the fluorite lattice structure of ceria had been preserved during the doping process. The ceria sample was prepared from a commercial ceria powder by the heat treatment; the fine ceria powder smaller than 325 mesh was sintered at 1200°C to obtain ceria particles of 80–120 mesh sizes. Further increase of the heat treatment temperature beyond 1200°C drastically decreased the surface area of ceria without affecting the crystal structure as evidenced by the X-ray diffraction analysis.

$Rh/Al_2O_3$, $Rh/CeO_2$, and $Rh/CeO_2$-*a* catalysts were prepared by impregnating the respective supports with $[(n-C_4H_9)_4N]_2[Rh(CO)Br_4]_2$. This nonaqueous impregnation technique (*28*) yielded a very shallow Rh metal band near the periphery of a catalyst particle. Following impregnation the catalysts were dried overnight in air at room temperature, heated slowly in flowing air to 500°C, and then held at that temperature for 4 h. The Rh dispersion, measured by $H_2$ chemisorption in a flow system, revealed significant differences in Rh dispersion on the different supports. The impregnation band widths, determined by scanning electron microprobe analysis, indicated that the impregnation depth of Rh in $CeO_2$-*a* is close to zero due to the nonporous nature of the modified ceria support. The detailed characteristics of the catalyst and the reactor are listed in Table 1; the reactor experiments followed the procedure described previously (*14*).

In standard cycling experiments a complete cycle was made of an NO half-cycle of 30 s duration, followed by a CO half-cycle

TABLE 1

Catalysts and Reactor Characteristics

| | | | | |
|---|---|---|---|---|
| | Supports | | | |
| Particle size | 80–120 mesh(125–177 $\mu$m diam.) | | | |
| BET surface area | 70 $m^2/g$ ($Al_2O_3$) | | | |
| | 0.3 $m^2/g$ ($CeO_2$) | | | |
| | 0.05 $m^2/g$ ($CeO_2$-*a*) | | | |
| Bulk density | 2.046 $g/cm^3$ ($Al_2O_3$) | | | |
| | 5.218 $g/cm^3$ ($CeO_2$) | | | |
| | 7.658 $g/cm^3$ ($CeO_2$-*a*) | | | |
| | Catalysts | | | |
| | Rh loading (wt %) | Sample weight (g) | Impregnation depth ($\mu$m) | Dispersion (%) |
| $Rh/Al_2O_3$ | 0.09 | 0.022 | 20 | 28 |
| $Rh/CeO_2$ | 0.04 | 0.049 | 30 | 12 |
| $Rh/CeO_2$-*a* | 0.04 | 0.049 | ~0 | 4 |
| | Reactor | | | |
| 0.32-cm-O.D. stainless-steel tubing: | | | | |
| Bed depth | 1 cm ($Rh/Al_2O_3$, $Rh/CeO_2$) | | | |
| | 0.7 cm ($Rh/CeO_2$-*a*) | | | |
| Gas flow rate | 50 $cm^3$/min (STP) | | | |
| Temperature | 200–500°C | | | |
| Pressure | 101.3 kPa (1 atm) | | | |

of 30 s duration. With regular reactants CO and NO, the reaction products $CO_2$ and $N_2O$ have the same mass number of 44, which cannot be separated mass spectroscopically. Thus, the $^{13}CO$ isotopic molecule was used in place of CO so that $^{13}CO_2$ (mass number = 45) could easily be separated from $N_2O$. The purity of $^{13}C$ atoms in $^{13}CO$ was 99%.

For simplicity in notation, CO is used for $^{13}CO$ and $CO_2$ for $^{13}CO_2$ throughout the paper. Note that the catalyst sample weights in Table 1 were chosen so that the total amount of the noble metal in the reactor is essentially the same in all cases. With very high space velocity and very small surface area of both the $CeO_2$ and $CeO_2$-*a* supports used in this study, the blank activity due to the reactor tube and the support material was negligible at 500°C for all three catalyst supports.

## RESULTS

### *Oxygen Storage Capacity of Supports*

In view of the importance of oxygen storage capacity of supports in determining the lifetime of Rh catalysts for NO decomposition as discussed earlier, we measured and compared the oxygen storage capacities of $Rh/Al_2O_3$, $Rh/CeO_2$, and $Rh/CeO_2$-*a* using a transient experimental technique. The comparison was based on an equal amount of catalyst sample by weight. We want to point out that the oxygen storage capacity of $CeO_2$ consists entirely of intrinsic oxygen vacancies, while that of $CeO_2$-*a* consists of both intrinsic and extrinsic oxygen vacancies. Thus it is useful to compare the oxygen storage capacity of $CeO_2$ with that of $CeO_2$-*a* for the same amount of each sample.

The population balance of total oxygen vacancy in $CeO_2$ and $CeO_2$-*a* can be written as

$$\delta \leq (1 - \alpha)\delta' + (1 - \alpha)\,\delta, \qquad (7)$$

for the solid-state reaction presented in Eq. (4). The left-hand side of Eq. (7) represents the intrinsic oxygen vacancy in reduced ceria, whereas the right-hand side represents the total (i.e., intrinsic and extrinsic) oxygen vacancy in the modified ceria. The first term of the rhs of Eq. (7) represents the extrinsic oxygen vacancy created in $(1 - \alpha)CeO_2$, while the second term represents the intrinsic oxygen vacancy in the reduced $(1 - \alpha)CeO_2$. By putting Eqs. (5) and (6) into Eq. (7) with the established knowledge of $\delta \leq 0.5$, we can show that the equality sign in Eq. (7) is valid for doubly charged oxygen vacancies with $\delta = 0.5$, while the inequality sign is for singly charged ones. Thus Eq. (7) indicates that the total number of oxygen vacancies in $CeO_2$-*a* cannot be less than that in the same amount of $CeO_2$.

In order to measure the oxygen uptake of the various supports, we carried out transient cycling experiments where pulses of $O_2$ and He were alternated with a cycling period of 20 s, after reducing the catalysts with $H_2$ at 500°C following the procedures described previously (*14*). That is, the reactor was fed with an oxygen pulse of 10 s duration containing 1.19 $\mu$mol of $O_2$, followed by a He pulse of 10 s duration which was followed by the next $O_2$ pulse and so

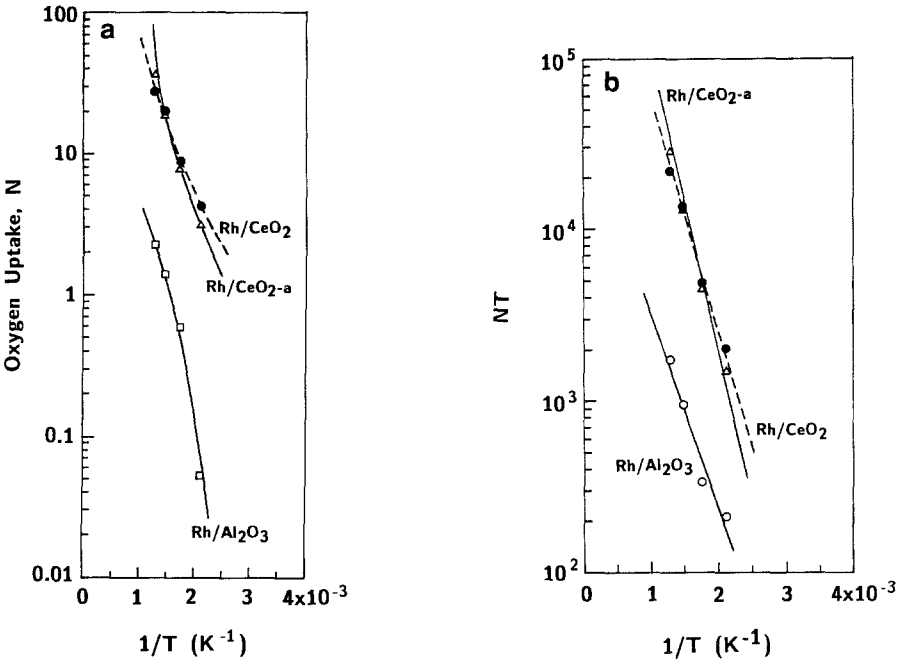


FIG. 2. (a) Total oxygen uptake measured by transient pulse experiments (□) $Rh/Al_2O_3$, (●) $Rh/CeO_2$, (Δ) $Rh/CeO_2$-*a*. (b) Activation energy for oxygen uptake (○) $Rh/Al_2O_3$, (●) $Rh/CeO_2$, (△) $Rh/CeO_2$-*a*.

on. The total oxygen uptake was calculated from the number of $O_2$ pulses disappeared before the breakthrough of the $O_2$ pulse occurs in this continuous cycling experiment. Note that the number of $O_2$ pulses required to reach a monolayer coverage of the Rh surface alone is approximately 0.08 pulse assuming 100% Rh dispersion.

In this type of transient experiment, the total oxygen uptake is controlled by the mobility of oxygen rather than by the oxygen-storage capacity. That is, the ultimate oxygen-storage capacity is not completely utilized because the oxygen mobility in the catalysts is slow compared to the time scale of the feedstream cycling. Therefore, the total oxygen uptake measured in this experiment is not the ultimate oxygen-storage capacity which is independent of temperature, but it is the amount of the utilized storage capacity which depends on the oxygen mobility which in turn depends upon the catalyst temperature.

Results shown in Fig. 2a indicate that the total oxygen uptake for $Rh/CeO_2$ and $Rh/CeO_2$-*a* is larger than that of $Rh/Al_2O_3$ by more than an order of magnitude. The oxygen uptake of $Rh/CeO_2$ is slightly larger than that of $Rh/CeO_2$-*a* in the low temperature regime of the experiments, while the reverse is true in the high temperature regime. The increase of oxygen uptake with temperature shown in Fig. 2a is indicative of the activated nature of the process. This is in accordance with earlier results, which showed that the kinetics of oxygen incorporation in the ceria structure is controlled by the oxygen anion mobility (*29*).

The kinetics of oxygen mobility in the crystal structure of ceria can be described by (*17, 20*)

$$\mu T = \mu_0 \exp(E/\mathrm{RT}), \qquad (8)$$

where $\mu$ is the oxygen mobility. When the oxygen uptake is controlled by the mobility of the oxygen anion, Eq. (8) can be written in terms of the oxygen uptake such as

$$NT \alpha \mu_0 \exp(E/\mathrm{RT}), \qquad (9)$$

TABLE 2

Activation Energy for Oxygen Uptake

| Catalysts | Activation energy |
|---|---|
| $Rh/Al_2O_3$ | 5.24 ± 0.29 kcal/mol |
| $Rh/CeO_2$ | 6.22 ± 0.27 |
| $Rh/CeO_2$-*a* | 8.02 ± 0.39 |

where $N$ is the total number of oxygen pulses taken up by the catalysts and thus disappeared before the breakthrough of oxygen during a pulse experiment. The activation energy of oxygen uptake, determined from the slope of the straight lines of the $\ln(NT)$ vs $1/T$ plots in Fig. 2b, is listed in Table 2. Note that the activation energy of oxygen uptake for $Rh/CeO_2$-*a* is 1.8 kcal/mol larger than that for $Rh/CeO_2$. This difference can be attributed to the associative defect–defect interaction between dopant cations and oxygen anions. In fact, the difference of 1.8 kcal/mol is in line with the reported value of 1.3 kcal/mol for this type of interaction (*18*).

*Transient Response of Supported Rh Catalysts at 500°C*

Transient responses of the Rh catalysts impregnated on the three different supports—$Al_2O_3$, $CeO_2$, and $CeO_2$-*a*—were compared for the NO + CO reaction at 500°C. Figures 3a through 3d present the detailed evolution pattern of transient responses as measured by the reactor outlet concentrations during symmetric composition-cycling experiments at a cycling period of 20 s. In these experiments, the feedstream composition was cycled between 800 ppm CO in He and 800 ppm NO in He. At room temperature (Fig. 3a) all three catalysts exhibit no activity for the NO + CO reaction. Figures 3b and through 3d were obtained at 500°C with $Rh/Al_2O_3$, $Rh/CeO_2$, and $Rh/CeO_2$-*a*, respectively. Comparison of Figs. 3b, 3c, and 3d shows that CO introduced during the CO half-cycle produces more $CO_2$ on $Rh/CeO_2$-*a* than on $Rh/CeO_2$ which in turn produces more $CO_2$ than $Rh/Al_2O_3$. Since there is no oxygen source during the CO half-cycle, the oxygen needed to produce $CO_2$ from CO must have been carried over from the previous NO half-cycle, where oxygen was produced from the decomposition of NO. Obviously, the oxygen storage capacity for this carryover must decrease in the following order; $Rh/CeO_2$-*a* > $Rh/CeO_2$ > $Rh/Al_2O_3$. This is consistent with the relative magnitudes of oxygen uptakes on these catalysts as shown in Fig. 2a. The absence of oxygen in the gas phase indicates that the oxygen produced from the NO decomposition accumulates on the catalysts.

For all three catalysts, NO decomposes to nitrogen and oxygen during the early part of the NO half-cycle, and the catalysts gradually lose their NO decomposition activity, as evidenced by the evolution of NO. This gradual loss of the NO decomposition activity of Rh occurs in 5, 7, and 9 s into the NO half-cycle for $Rh/Al_2O_3$, $Rh/CeO_2$, and $Rh/CeO_2$-*a*, respectively. This means that, for transient NO decomposition, $Rh/CeO_2$-*a* can sustain the catalytic activity of Rh for a longer period than $Rh/CeO_2$ which in turn can sustain it for a longer period than $Rh/Al_2O_3$. As a result, the nitric oxide introduced during the NO half-cycle can produce more nitrogen on $Rh/CeO_2$-*a* than on $Rh/CeO_2$, which in turn can produce more nitrogen than $Rh/Al_2O_3$, as can be seen in Figs. 3b through 3d. This is in complete correspondence with the $CO_2$ production during the CO half-cycle.

The time-average conversion of NO determined from Figs. 3b through 3d are listed in Table 3 for $Rh/Al_2O_3$, $Rh/CeO_2$, and $Rh/CeO_2$-*a*; it indicates that a significant improvement in the overall performance of Rh can be achieved at high temperatures by the use of $CeO_2$ or $CeO_2$-*a* in place of $Al_2O_3$. Furthermore, if we take into account the fact that $Rh/CeO_2$-*a* has much lower Rh dispersion than $Rh/Al_2O_3$, the enhancement of specific Rh activity (i.e., Rh activity per Rh site) would be expected to be even more significant than what is indicated in Table 3. It thus appears reasonable to conclude that

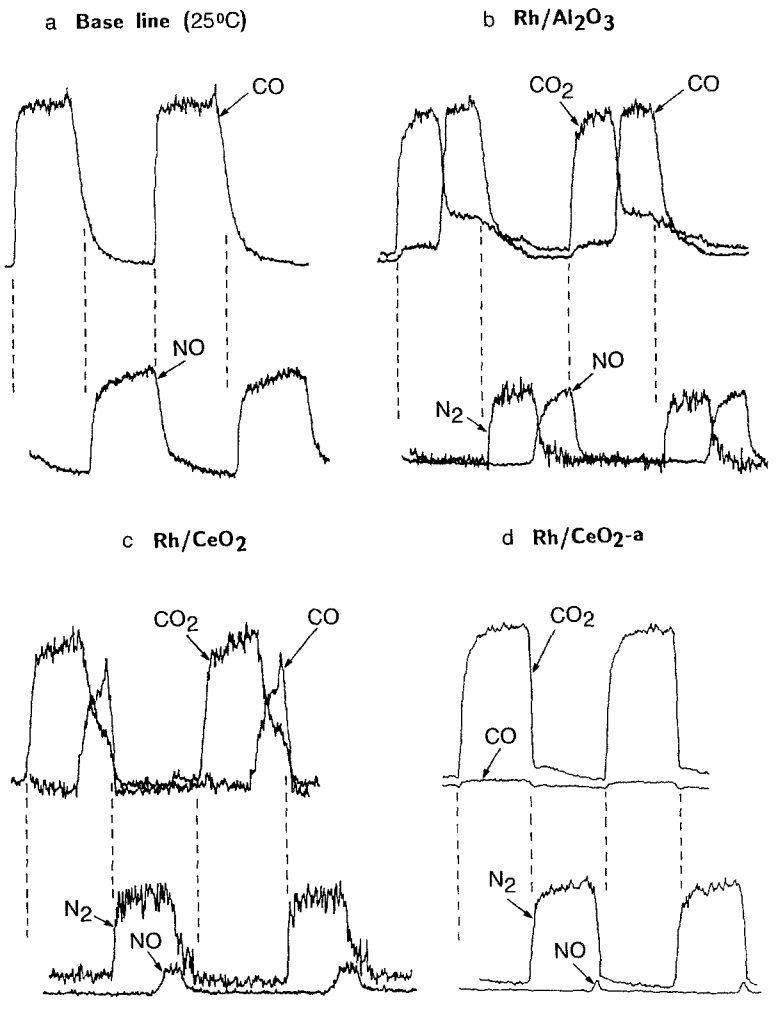


FIG. 3. Time variations of the reactor outlet concentrations during symmetric cycling operation over supported Rh catalysts. (a) $T$ = 25°C, (b) $T$ = 500°C; cycling period = 20 s. (c,d) $T$ = 500°C, cycling period = 20 s.

the modified ceria support developed in this work is superior to the conventional ceria or alumina as a catalyst support for Rh during the NO + CO reaction under cycled operating conditions employed in this work at high temperatures.

Figures 4a through 4d were obtained from symmetric cycling experiments with a cycling period of 60 s while keeping all other conditions the same as those used for Figs. 3a through 3d, respectively. The performance of $Rh/CeO_2$-*a* is shown again to be superior to that of $Rh/Al_2O_3$ and $Rh/CeO_2$. The time-average conversion of NO determined from Figs. 4b through 4d is also listed in Table 3. Cross-column comparison of the NO conversion levels in Table 3 indicates that $Rh/CeO_2$-*a* can tolerate a longer cycling period for a given performance requirement

TABLE 3

Cycled Performance of Rh Catalysts ($T$ = 500°C)

| | Cycling period = 20 s | Cycling period = 60 s |
|---|---|---|
| $Rh/Al_2O_3$ | 76.5% | 50.8% |
| $Rh/CeO_2$ | 86.5% | 57.8% |
| $Rh/CeO_2$-*a* | 98.2% | 82.5% |

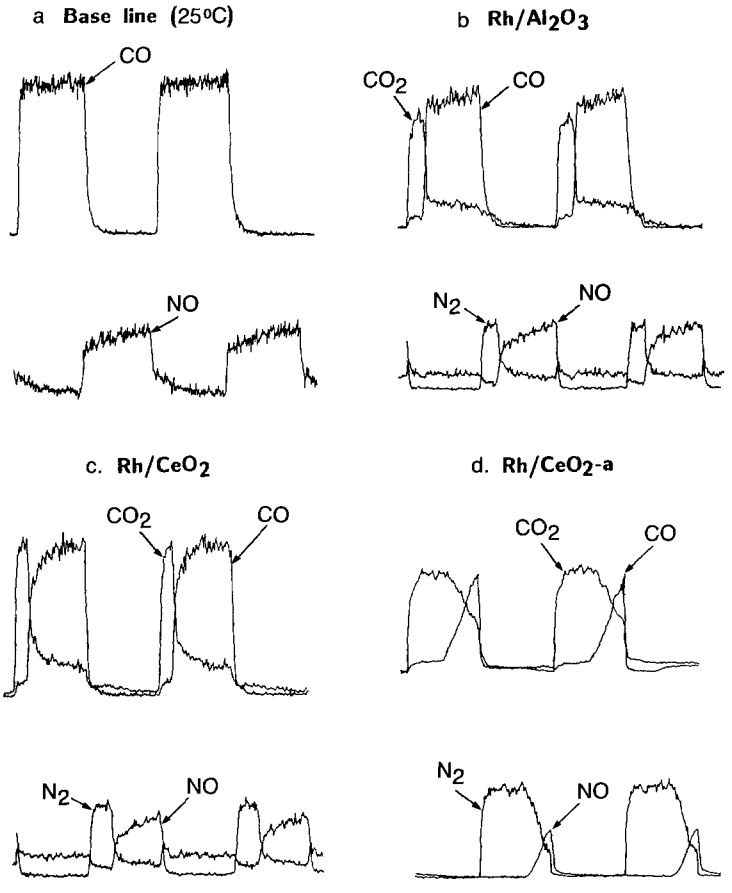


FIG. 4. Time variations of the reactor outlet concentrations during symmetric cycling operation over supported Rh catalysts (a) $T$ = 25°C, (b) $T$ = 500°C; cycling period = 60 s. (c,d) $T$ = 500°C, cycling period = 60 s.

than either $Rh/Al_2O_3$ or $Rh/CeO_2$ can. For example, in order to achieve an NO conversion greater than 75%, the cycling period must be shorter than 20 s for $Rh/Al_2O_3$ whereas a cycling period of 60 s is still acceptable for $Rh/CeO_2$-*a*. This improved tolerance of $Rh/CeO_2$-*a* toward longer cycling periods can be attributed to the large oxygen storage capacity of $CeO_2$-*a* compared with those of $CeO_2$ and $Al_2O_3$ at 500°C as shown in Fig. 2, and suggests the possibility of widening the window of $A/F$ ratio control for three-way catalysts without significantly sacrificing the cycled performance.

### *Effect of Temperature on the Cycled Performance of Rh*

So far we have shown that the transient catalytic activity of Rh at 500°C under cycled operating conditions can be significantly enhanced by chemical modification of the support. Now we examine the effect of catalyst temperature on the cycled performance of the supported Rh catalysts. Figures 5a and 5b present the effect of catalyst temperature on the performance of the $Rh/Al_2O_3$, $Rh/CeO_2$, and $Rh/CeO_2$-*a* catalysts when the feedstream composition was cycled between 800 ppm CO and 800 ppm NO with cycling periods of 20 s and 60 s, respectively. Data points represent the time-average NO conversion averaged over a few experimental runs. Both figures indicate that at temperatures above 475°C $Rh/CeO_2$-*a* performs better than $Rh/CeO_2$, which in turn performs better than $Rh/Al_2O_3$, whereas below 400°C $Rh/Al_2O_3$ outperforms both $Rh/CeO_2$ and $Rh/CeO_2$-*a*. It seems reasonable

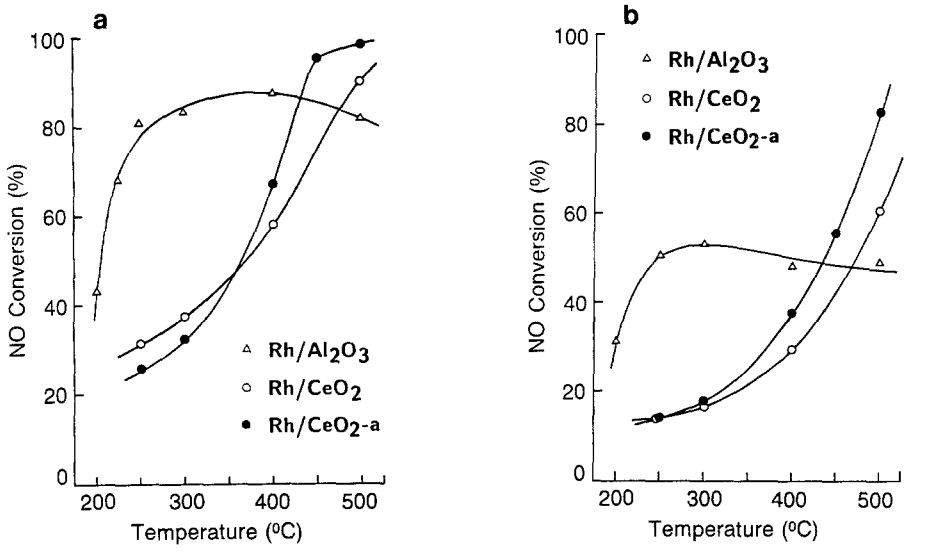


FIG. 5. Effect of temperature on the cyclic performance of supported Rh symmetric cycling, (a) cycling period = 20 s, (b) cycling period = 60 s.

at this point to speculate that the superior performance of $Rh/Al_2O_3$ at low temperatures may be attributable to its larger surface area of Rh. In fact, the order of the low temperature performance, namely

$$Rh/Al_2O_3 > Rh/CeO_2 > Rh/CeO_2\text{-}a, \quad (10)$$

is the same as the order of the Rh dispersion. It is remarkable, however, that this order completely reverses at high temperatures to

$$Rh/Al_2O_3 < Rh/CeO_2 < Rh/CeO_2\text{-}a, \quad (11)$$

despite the fact that Rh dispersion on $CeO_2$-*a* is only one-seventh that on $Rh/Al_2O_3$. Obviously, this phenomenon cannot be explained simply by the difference in either Rh dispersion or Rh particle size. It cannot be explained by the effect of ceria on the kinetics of NO + CO reaction reported recently by Oh (*12*) either. As we have shown earlier, this can be explained by the oxygen storage capacity of the support.

Comparison of the high temperature performance in Fig. 5a with that in Fig. 5b shows that the enhancement of transient Rh activity due to $CeO_2$ and $CeO_2$-*a* supports becomes more pronounced when the cycling period becomes longer. This may be explained in light of the oxygen storage capacity as follows: The NO decomposition during the longer NO half-cycle leads to the accumulation of more oxygen which deactivates the catalytic activity. Consequently, the oxygen storage capacity of the catalyst support becomes more important for the longer NO half-cycle.

### *Effect of Temperature on the Steady-State Performance of Rh*

In the previous section we explained the differences in the low temperature cycled performance among $Rh/Al_2O_3$, $Rh/CeO_2$, and $Rh/CeO_2$-*a* in terms of Rh dispersion. This seems reasonable in view of the fact that the oxygen mobility at low temperatures may not be fast enough to influence the rate of the NO + CO reaction. However, we cannot completely rule out the possibility of some kinetic effects of Ce on the NO + CO reaction over Rh, similar to those observed by Oh (*12*) under steady-state conditions.

In order to check the significance of this possibility, the steady-state performances of the Rh catalysts impregnated on the three different supports—$Al_2O_3$, $CeO_2$, and $CeO_2$-*a*—were compared for the NO + CO

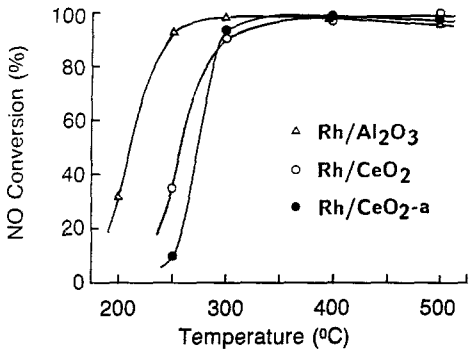


FIG. 6. Effect of catalyst temperature on the steady-state performance of supported Rh catalysts.

reaction over the temperature range of 200–500°C in a feed stream containing 800 ppm CO and 800 ppm NO in He. In this comparison we point out that the three catalysts—$Rh/Al_2O_3$, $Rh/CeO_2$, and $Rh/CeO_2$-*a*—have different Rh surface area due to their different Rh dispersion, as shown in Table 1.

It is seen in Fig. 6 that there are significant differences among these catalysts in the lightoff temperature for NO conversion: $Rh/Al_2O_3$ lights off at approximately 210°C, $Rh/CeO_2$ at 250°C, and $Rh/CeO_2$-*a* at 265°C. These differences can be explained by the difference in Rh dispersion, details of which can be found in the Appendix A. That is, the high lightoff temperature for $Rh/CeO_2$-*a* compared with that for $Rh/Al_2O_3$ can be attributed to the low Rh surface area on $Rh/CeO_2$-*a* compared with that on $Rh/Al_2O_3$. This means that, under the conditions of our experiments, the kinetic effects of ceria on the NO + CO reaction over Rh is not significant in the low temperature regime. This also supports our earlier speculation that the relatively poor cycled performance of $Rh/CeO_2$-*a* in the low temperature regime is due primarily to its low Rh surface area, even though there may exist some kinetic effects caused by ceria.

## DISCUSSION

In this work we have demonstrated that the catalytic activity of Rh for the NO + CO reaction under warmed-up cycled feedstream conditions can be significantly improved by modifying the oxygen transport and storage characteristics of the catalyst support. Specifically, we have shown that, at high temperatures around 500°C, $Rh/CeO_2$-*a* exhibits the best cycled performance followed by $Rh/CeO_2$ and $Rh/Al_2O_3$. This order is shown to be completely reversed at low temperatures. The superior performance of $Rh/CeO_2$-*a* at high temperatures can be attributed to the improved oxygen storage/transport characteristics in the support, whereas the poor performance of $Rh/CeO_2$-*a* at low temperatures can be attributed to the low dispersion of Rh on $CeO_2$-*a*. It appears reasonable to speculate that the performance of $Rh/CeO_2$-*a* at low temperatures can be readily improved either by developing a high surface $CeO_2$-*a* on which impregnation of Rh with high dispersion can be achieved or by coimpregnating Ce and Gd on an $Al_2O_3$ support followed by proper calcination to make $CeO_2$-*a* on the support. We are currently working on this.

It was shown in Fig. 2a that $Rh/CeO_2$-*a* can take up more oxygen than $Rh/CeO_2$ at high temperatures even though this trend reverses at low temperatures. This can be explained as follows. At low temperatures (below 300°C) where oxygen mobility is rather slow (*30*), the oxygen uptake occurs only in a thin shell near the external surface of individual support particles in their state of aggregation. This means that the oxygen uptake depends on both the oxygen mobility and the BET surface area of the support. When the difference in the oxygen mobility between the two samples is not significant at low temperatures, the BET surface area becomes more important than the oxygen mobility in determining the total amount of the oxygen uptake. Thus, $Rh/CeO_2$ can take up more oxygen than $Rh/CeO_2$-*a* at low temperatures since $CeO_2$ has a larger BET surface area than $CeO_2$-*a*. At high temperatures (above 400°C) where oxygen mobility is fairly large (*26*), the oxygen uptake can occur in a wide shell close to the center of

the individual support particles. This means that the total number of oxygen vacancies becomes a dominating factor that influences the oxygen uptake at high temperatures. Thus, $Rh/CeO_2$-*a* can take up more oxygen than $Rh/CeO_2$ at high temperatures because $CeO_2$-*a* can have more oxygen vacancies that $CeO_2$, as discussed earlier. This explanation is consistent with the cycled performance of Rh observed in Figs. 5a and 5b. It should be noted here that the effects of both the BET surface area and the total number of oxygen vacancies on the oxygen uptake discussed above do not affect in any way the validity of either Eq. (9) or Fig. 2b in measuring the activation energy of the oxygen uptake in a given sample where both the BET surface area and the total number of oxygen vacancies remain constant during the oxygen uptake measurements at different temperatures.

In agreement with our previous study (*14*), we consistently observed $N_2O$ formation during the NO + CO reaction over all three catalysts we studied, details of which will be reported in a subsequent paper.

## SUMMARY AND CONCLUSIONS

Oxygen storage and transport characteristics of a ceria support were chemically modified by doping with gadolinia. Transient oxygen uptakes as well as catalytic activities of Rh supported on this modified ceria were measured and compared with those of Rh supported on ceria or alumina. Major findings of this study are:

1. The oxygen uptakes of both ceria and modified ceria are an order of magnitude greater than that of alumina.

2. The activation energy for oxygen uptake increases in the order

$$Rh/Al_2O_3 < Rh/CeO_2 < Rh/CeO_2\text{-}a.$$

3. The chemical modification of the ceria support can significantly enhance the transient catalytic activity of Rh for the NO + CO reaction under cycled feedstream conditions. More specifically, at high temperatures above 500°C the cycled performance of the Rh catalysts for the NO + CO reaction improves in the order

$$Rh/Al_2O_3 < Rh/CeO_2 < Rh/CeO_2\text{-}a.$$

4. The difference in transient catalytic activity of Rh can be attributed to the difference in oxygen storage and transport characteristics over the various supports.

These findings suggest that there is a strong possibility of reducing the Rh usage requirement in three-way catalytic converters by improving the oxygen storage and transport characteristics of the catalysts through the chemical modification of the supports.

## APPENDIX A: EFFECT OF Rh DISPERSION ON REACTION LIGHTOFF TEMPERATURE

We examine the effect of Rh dispersion on the reaction lightoff temperatures for the NO + CO reaction over $Rh/Al_2O_3$, $Rh/CeO_2$, and $Rh/CeO_2$-*a* under steady-state conditions, for these catalysts have different levels of Rh dispersion. A steady-state mass balance for NO in a plug flow reactor yields

$$\varepsilon V \frac{dC}{dz} = -\sigma \tilde{R}, \qquad \text{(A.1)}$$

where $\tilde{R}$ is the rate of the NO + CO reaction. Since $\tilde{R}$ is controlled by the rate of NO decomposition at temperatures below the reaction lightoff temperature (*14*), it can be written in terms of the NO decomposition rate. That is,

$$\tilde{R} = k(T) f(C), \qquad \text{(A.2)}$$

where $k$ is the rate constant for the NO decomposition which depends on temperature, and $f$ is the rest of the rate expression which depends on the composition. Note that $f$ can be expressed as a function of NO concentration alone, since at steady state the CO concentration can be expressed in terms of the NO concentration in this bimolecular reaction (cf. *31*). In fact, this form of the rate expression [Eq. (A.2)] was successfully applied to the NO + CO reaction by Hecker and Bell (*32*) to fit their experimental

data. Combining Eqs. (A.1) and (A.2) followed by integration, we get

$$\tau k = \int_{C_o}^{C_i} \frac{dC}{f(C)}, \qquad \text{(A.3)}$$

where $C_i$ and $C_o$ are the reactor inlet and outlet concentration of NO and $\tau$ is a constant defined by

$$\tau = \sigma L/\varepsilon V \qquad \text{(A.4)}$$

and is a measure of residence time. If we assume that the intrinsic kinetic expressions are independent of Rh particle size, the rate expression $f(C)$ should be identical for all three catalysts. This means in Eq. (A.3) that the NO conversion depends only on $\tau k$ provided the inlet NO concentration is kept constant for all catalysts. In other words, $\tau k$ must be kept constant to achieve the same NO conversion. It is useful to note here that $\tau$ is proportional to the Rh dispersion when other conditions are the same. Thus, if the reaction lightoff temperature for $Rh/Al_2O_3$ is 210°C as shown in Fig. 3a, the reaction lightoff temperatures for $Rh/CeO_2$ and $Rh/CeO_2$-*a* can be estimated to be 232 and 263°C, respectively, from the reaction

$$(\tau k)_1 = (\tau k)_2 = (\tau k)_3 \qquad \text{(A.5)}$$

at the 50% conversion level. In the above equation the subscripts 1, 2, and 3 denote $Rh/Al_2O_3$, $Rh/CeO_2$, and $Rh/CeO_2$-*a*, respectively, and an activation energy of 19 kcal/mol was used for $k$ (*33*). The above analysis indicates that the difference in the reaction lightoff temperature among the different catalysts shown in Fig. 3a can be explained reasonably well by the difference in Rh dispersion.

## APPENDIX B: NOMENCLATURE

$C$ gas phase concentration of NO in Eq. (A.1), mol/cm$^3$
$C_i$ NO concentration in the reactor inlet in Eq. (A.3), mol/cm$^3$
$C_o$ NO concentration in the reactor outlet in Eq. (A.3), mol/cm$^3$
$C_{CO}$ feed concentration of CO, ppm
$C_{NO}$ feed concentration of NO, ppm
$Ce_{Ce}$ Ce cation on a regular Ce site in ceria lattice
$E$ activation energy for oxygen mobility, cal/mol
$f$ composition dependency in the rate expression of Eq. (A.2)
$k$ rate constant for NO decomposition, mol/cm$^2$ · s
$L$ total reactor length, cm
$M$ trivalent dopant cation
$M_{Ce}$ trivalent dopant cation on a regular Ce site in ceria lattice
$N$ total number of oxygen pulses taken up by the catalysts and thus disappeared from the reactor effluent during the pulse experiments
$R$ reductant
$R_g$ gas constant
$\tilde{R}$ rate of the No + CO reaction, mol/cm$^2$ · s
$V$ superficial linear gas velocity, cm/s
$V_O$ oxygen ion vacancy
$T$ absolute temperature, K
$z$ axial distance along the reactor, cm

*Greek Letters*

$\alpha$ stoichiometry number in the solid state reaction of Eq. (4)
$\delta$ number of intrinsic oxygen vacancies per Ce in modified ceria
$\delta'$ number of extrinsic oxygen vacancies per Ce in modified ceria
$\varepsilon$ void fraction of the reactor bed
$\mu$ oxygen mobility, mol/s
$\mu_O$ preexponential factor for oxygen mobility, mol · K/s
$\sigma$ catalytic surface area, cm$^2$/cm$^3$ reactor
$\tau$ specific residence time defined by Eq. (A.4), s/cm

## ACKNOWLEDGMENTS

The author gratefully acknowledges C. J. Stock for his contribution during the early stage of this work, M. J. D'Aniello, Jr. for his guidance in catalyst impreg-

nation techniques, and J. L. Johnson (Analytical Chemistry Department) for his X-ray diffraction analysis of the catalyst samples.

## REFERENCES


1. Taylor, K. C., *in* "Catalysis: Science and Technology" (J. R. Anderson and M. Boudart, Eds.), Vol. 5. Springer-Verlag, Berlin, 1984.
2. Adams, K. M., and Gandhi, H. S., *Ind. Eng. Chem. Prod. Res. Dev.* **22,** 207 (1983).
3. Yokoda, K., Muraki, H., and Fujitani, Y., SAE Paper 850129, 1985.
4. Muraki, H., Shinjoh, H., and Fujitani, Y., *Appl. Catal.* **22,** 325 (1986).
5. Cho, B. K., *Ind. Eng. Chem. Res.* **27,** 30 (1988).
6. Gandhi, H. S., Piken, A. G., Shelef, M., and Delosh, R. G., SAE Paper 760201, 1976.
7. Schlatter, J. C., and Mitchell, P. J., *Ind. Eng. Chem. Prod. Res. Dev.* **19,** 288 (1980).
8. Herz, R. K., and Sell, J. A., *J. Catal.* **94,** 166 (1985).
9. Harrison, B., Diwell, A. F., and Hallett, C., *Platinum Metals Rev.* **32,** 73 (1988).
10. Kummer, J. T., Yao, Y., and McKee, D., SAE Paper No. 760143 (1976).
11. Oh, S. H., and Eickel, C. C., *J. Catal.* **112,** 543 (1988).
12. Oh, S. H., *J. Catal.* **124,** 477 (1990).
13. Cho, B. K., and Stock, C. J., presented at the 1986 Annual Meeting of American Institute of Chemical Engineers, Miami Beach, FL, Nov. 1986.
14. Cho, B. K., Shanks, B. H., and Bailey, J. E., *J. Catal.* **115,** 486 (1989).
15. Summers, J. C., and Ausen, S. A., *J. Catal.* **58,** 131 (1979).
16. Herz, R. K., *Ind. Eng. Chem. Prod. Res. Dev.* **20,** 451 (1981).
17. Tuller, H. L., and Nowick, A. S., *J. Electrochem. Soc.* **122,** 255 (1975).
18. Tuller, H. L., and Nowick, A. S., *J. Electrochem. Soc.* **126,** 209 (1979).
19. Kroger, F. A., "The Chemistry of Imperfect Crystals," Vol. 2. North-Holland, Amsterdam, 1974.
20. Etsell, T. H., and Flengas, S. N., *Chem. Rev.* **70,** 339 (1970).
21. Wang, D. Y., and Nowick, A. S., *Solid State Ionics* **5,** 551 (1981).
22. Butler, V., Catlow, C. R. A., Fender, B. E. F., and Harding J. H., *Solid State Ionics* **8,** 109 (1983).
23. Gerhardt-Anderson, R., and Nowick, A. S., *Solid State Ionics* **5,** 547 (1981).
24. Wang, D. Y., Park, D. S., Griffith, J., and Nowick, A. S., *Solid State Ionics* **2,** 95 (1981).
25. Kilner, J. A., *Solid State Ionics* **8,** 201 (1983).
26. Bevan, D. J. M., and Summerville, E., *in* "Handbook on the Physics and Chemistry of Rare Earths" (K. A. Gschneidner, Jr. and L. Eyring, Eds.), Vol. 3. North-Holland, Amsterdam, 1979.
27. Kilner, J. A., and Brook, R. J., *Solid State Ionics* **6,** 237 (1982).
28. D'Aniello, M. J., U.S. Patent 4,380,510 (1983).
29. Mackrod, W. C., and Stewart, R. F., *J. Phys. C: Solid State Phys.* **12,** 5015 (1979).
30. Eyring, L., *in* "Handbook on the Physics and Chemistry of Rare Earths" (K. A. Gschneidner, Jr. and L. Eyring, Eds.), Vol. 3. North-Holland, Amsterdam, 1979.
31. Prairie, M. R., Cho, B. K., Oh, S. H., Shinouskis, E. J., and Bailey, J. E., *Ind. Eng. Chem. Res.* **27,** 1396 (1988).
32. Hecker, W. C., and Bell, A. T., *J. Catal.* **84,** 200 (1983).
33. Oh, S. H., Fisher, G. B., Carpenter, J. E., and Goodman, D. W., *J. Catal.* **100,** 360 (1986).